Journal of Visualized Experiments

Bead movement based computational framework for 3-dimensional analysis of biofilm material heterogeneity
--Manuscript Draft--

Article Type:	Invited Methods Article - JoVE Produced Video
Manuscript Number:	JoVE62454R3
Full Title:	Bead movement based computational framework for 3-dimensional analysis of biofilm material heterogeneity
Corresponding Author:	Bettina Buttaro Lewis Katz School of Medicine Temple University Philadelphia, PA UNITED STATES
Corresponding Author's Institution:	Lewis Katz School of Medicine Temple University
Corresponding Author E-Mail:	bbuttaro@temple.edu
Order of Authors:	Bettina Buttaro
	Gillian Queisser

Additional Information:	
Question	**Response**
Please indicate whether this article will be Standard Access or Open Access.	Open Access (US$4,200)
Please specify the section of the submitted manuscript.	Biology
Please indicate the **city, state/province, and country** where this article will be **filmed**. Please do not use abbreviations.	Philadelphia, Pennsylvania, United States of America
Please confirm that you have read and agree to the terms and conditions of the author license agreement that applies below:	I agree to the Author License Agreement
Please provide any comments to the journal here.	
Please indicate whether this article will be Standard Access or Open Access.	Open Access ($3900)

1 **TITLE:**
2 A Bead Movement Based Computational Framework for 3-Dimensional Analysis of Biofilm
3 Material Heterogeneity
4
5 **AUTHORS AND AFFILIATIONS:**
6 Bettina Buttaro[1], Gillian Queisser[2]
7
8 1.   Sol Sherry Thrombosis Research Center, Lewis Katz School of Medicine, Temple
9 University, Philadelphia, PA, USA
10 2.   Department of Mathematics, Temple University, Philadelphia, PA, USA
11
12 Bettina Buttaro, bbuttaro@temple.edu
13 Gillian Queisser, gillian.queisser@temple.edu
14

19 **SUMMARY:**
20 We describe a method for analyzing and quantifying the movement pattern of 1 μm
21 carboxylate beads through heterogeneous bacterial biofilms. Comparison of the movement
22 patterns can be used to quantitate differences in material properties of biofilms.
23

24 **ABSTRACT:**
25 Differences in the material properties of bacterial biofilms have been observed in biofilms of
26 different bacterial species, within the same species under different growth conditions and
27 after treatment with matrix modifying molecules. To better quantitate the material
28 properties of 3D biofilms, an experimental and computational workflow was developed and
29 applied to examine differences between *Enterococcus faecalis, Salmonella enterica* serotype
30 Typhimurium and *Escherichia coli* biofilms as well as the role of the amyloid curli in confirming
31 rigidity to Enterobacteriaceae biofilms. The spatio-temporal dynamics of 1 μm carboxylate
32 beads in biofilms were tracked in 20 μm 3D biofilms over 20 minutes. The 4D image stacks
33 were processed using the Mosaic plugin in ImageJ to produce 3D trajectory data of bead
34 movement. This trajectory data was analyzed with a newly developed Bead Evaluator toolbox,
35 where movement data, including trajectory lifespans, bead velocities, cell densities along
36 trajectories, and bounding box information were computed and stored in csv-files. This paper
37 presents the workflow from experimental setup and image recording to bead trajectory
38 computation and analysis. The structure of curli-containing biofilms resulted in more stable
39 bead interactions and less bead movement than in curli-mutant and Enterococcal biofilms.
40 Bead movement did not appear strongly dependent on cell density when measuring the bead
41 velocity and trajectory bounding box volume, supporting the hypothesis that other material
42 properties of the biofilms control the bead dynamics. This technique is widely applicable to
43 quantitating differences in biofilms of different matrix compositions as well as biofilms before
44 and after matrix-modifying treatments.
45

46 **INTRODUCTION:**

47 Bacterial biofilms are ubiquitous as part of human microbiota and continuously interact with
48 molecules. These molecules range in size from 1 nm antibiotics and 1-3 mm bacteria to larger
49 particles of fiber in the gastrointestinal tract. The composition of single- or multispecies
50 biofilms affects the material properties and thus the movement pattern of particles through
51 biofilms[1-5]. One example is bacterial amyloids, which have a conserved, fibrillar cross-beta
52 sheet structure[6]. Amyloid curli is expressed by enteric bacteria such as *Escherichia coli* and
53 *Salmonella enterica* serotype Typhimurium and genes have been detected in multiple other
54 bacterial phylum[7]. Various material properties of biofilms are affected by curli[8,9]. Curli directly
55 interacts with other components of the matrix such as extracellular DNA (eDNA) and
56 cellulose[10,11]. Curli surrounds the cells and affects cellular membrane rigidity[12] and the overall
57 viscoelastic properties of the biofilm[13]. Curli mediates increased tensile strength by binding
58 to fibronectin, resulting in an increase in strong glass-surface attachment[14]. Incoming
59 bacteriophages bind to curli and limit phage invasion into biofilms[15].
60
61 When using multitest coated well slides to analyze roughly 20 µm thick *Enterococcus faecalis*,
62 *E. coli*, and *S.* Typhimurium biofilms using confocal microscopy, clear differences between *E.*
63 *coli*, *S.* Typhimurium[10,16] and *E. faecalis* biofilms (current study) could be observed. While
64 *Enterobacteriaceae* species biofilms had a high level of rigidity and areas with low cellular
65 density were easy to image, obtaining clear high-resolution pictures of *E. faecalis* biofilms
66 using line and frame averaging required the application of pressure to the slide to induce
67 sufficient surface tension for cell stability during the imaging process. Bacterial amyloids such
68 as curli form highly ordered structures, suggesting they may be relatively rigid[17]. This
69 motivated the hypothesis that amyloid curli could be inducing rigidity in *E. coli* and *S.*
70 Typhimurium biofilms. There was no clear evidence that *E. faecalis* was expressing amyloids
71 under the conditions studied. The protein Esp, a pilin gene associated with more pathogenic
72 strains of *E. faecalis*, was recently shown to produce amyloid structures[18]; however, using
73 blastn and blastp searches, this gene was not detected in the *E. faecalis* commensal type
74 strain OG1RF used in these studies. The pheromone cOB1, produced by OG1RF, can form
75 amyloid-like structures[19]. However, with the given biofilm growth conditions and amyloid
76 detection methods previously used for *S.* Typhimurium amyloid staining[10] in *E. faecalis,*
77 OG1RF amyloids could not be detected (data not shown). A new four-dimensional (4D) image
78 technique was developed to compare the overall material properties amongst the viscous *E.*
79 *faecalis*, *E. coli* and *S.* Typhimurium as well as to determine the contribution of amyloid to
80 Enterobacteriaceae biofilms using amyloid mutants of *S.* Typhimurium and *E. coli*.
81
82 In the past, fluorescent beads were successfully used to analyze the material properties of
83 biofilms in two dimensions (2D) using microrheology[20-25]. This can be applied to a three-
84 dimensional biofilm by studying 2D optic slices at various depths in the biofilm[26]. The current
85 technique was developed to track 1 µm microscale beads in 3D over time for use in 4D
86 modeling. Part of the rationale was the overarching concept of using 4D modeling to
87 understand movement of plasmids through gastrointestinal microbiota communities.
88 Fluorescently charged carboxylate beads with a 1 µm diameter were used since these
89 correspond well, with respect to size and charge, to *E. faecalis,* the chosen model organism
90 for plasmid movement and maintenance[27, 28]. A 4D assay to quantify the physical properties
91 of biofilms was developed (**Figure 1A**). In the devised methodology, beads were added to
92 biofilms and their spatio-temporal trajectories were recorded through 10-20 µm thick
93 biofilms over the course of 10-20 minutes. Bead trajectories in 3D were then quantified in

94 terms of trajectory length, bead velocity, trajectory bounding box volume (minimal box
95 containing the trajectory), and bounding box cellular density using a newly developed
96 toolbox. The following protocol can be employed to generate 4D image data of bacteria and
97 bead containing biofilms, to preprocess the data with ImageJ[29] and the plugin Mosaic, and to
98 analyze bead trajectories with a Bead Evaluator toolbox.

100 This technique has multiple applications for examining material properties as well as tracking
101 particle and bacterial movement in three dimensions. For example, an early version of this
102 technique was used to characterize the effect of monoclonal antibodies directed against curli
103 on the structural integrity of biofilms[16]. The full version has multiple tools to provide a more
104 detailed analysis of the biofilm material properties and is continuing to be used to examine
105 effects of monoclonal antibody treatment on biofilms. Particles of different charges can be
106 used to examine the material charge properties of the biofilms and movement of particles
107 through biofilms with different matrix compositions. This could be used to compare the
108 results from 2D microrheology that reveal the material properties responsible for movement
109 of beads we observed in biofilms that were not under flow. This technique could also be used
110 on mixed species biofilms with regions of different biofilm composition. Biofilms can be live
111 imaged under flow in microfluidic devices and flow cells to examine changes in the material
112 properties between static and flow biofilms as well as the effect of flow on movement of
113 particles. The techniques can also be applied to fluorescently labeled bacteria to characterize
114 the movement of exogenous bacteria through a biofilm community. Using three colors,
115 fluorescently labeled donor bacteria, fluorescently labelled recipient bacteria and
116 fluorescently labeled plasmids could be used to track movement, docking, and transfer of
117 plasmids.

119 **PROTOCOL:**

121 **1.   Biofilm preparation**

123 NOTE: Biofilms for analysis can be grown using any method that allows the biofilm to form on
124 an optic glass surface. The biofilm structure should adhere to the optic surface enough that
125 the structure is not disrupted during washing and/or mounting steps of the protocol. Below
126 describes the technique for 96-well optic bottom plates and 12 mm glass coverslips in 24-well
127 plates. Other options include different sized optic bottom plates and optic flow chambers
128 with and without flow.

130 1.1.   Biofilm setup

132 1.1.1.   Add bacterial growth medium to the wells of the plate. For this study, for *E.* faecalis,
133 add 2 mL of Todd-Hewitt (TH) to a 24-well plate and add 0.4 mL of TH to optic bottom 96-well
134 plates. For *S.* Typhimurium, *E. coli* and the isogenic *csgAB* curli mutants, add 0.7 mL of no-salt
135 Luria Broth (LB) to the wells. If using optic bottom chambers proceed to Step 1.2.

137 1.1.2.   Place 12 mm #1.5 glass optic coverslips in a Petri dish and cover them with ethanol.

139 1.1.3.   Using forceps, remove the coverslip and use a flame to light the remaining alcohol on
140 fire. Allow the alcohol to burn off. Just use the flame to light them on fire; do not hold the

141 coverslip in the flame because it will crack. Allow the coverslip cool for 10-20 s before placing
142 it in the well to prevent cracking.
143
144 1.1.4.   Place the coverslip into the well containing the medium at an angle to prevent it from
145 laying on top of the medium. Do not add the coverslip to a dry well and then add medium
146 because this will cause the coverslip to stick to the bottom of the well.
147
148 1.1.5.   Use a sterile pipette tip to carefully push the coverslip to the bottom of the well
149 containing the medium.
150
151 NOTE: Remember to match the thickness (#1 or #1.5) of the optic glass coverslip or optic
152 bottom plate to the thickness of the confocal microscope optics.
153
154 1.2.   Incubate the biofilm under proper conditions for biofilm growth. In these studies,
155 grow *E. faecalis* biofilms aerobically at 37 °C and grow *E. coli* biofilms aerobically at 30 °C.
156
157 1.2.1.   In these studies, grow *E. faecalis* biofilms for 2 days with medium switches in the
158 morning and early evening. To prevent damaging or dislodging the biofilm, carefully slant the
159 plate. Place the pipette tip near the bottom edge of the well and slowly draw out the medium.
160 Add the first mL of fresh medium in the same fashion. Add the second mL slowly near the
161 medium/well interface.
162
163 1.2.2. In these studies, use growth conditions for optimal curli production. Grow *S.*
164 Typhimurium biofilms at 28 °C for 6-8 days incubated on a slant that allowed the biofilm to
165 attach around 2/3 of the way up the slide and then grow as a pellicle on the air-liquid
166 interface. This was done without a medium change. To prevent the medium from drying out,
167 place the 24-well plate in a chamber with a water pan.
168
169 **2.   4D imaging**
170
171 2.1.   Preparation of the biofilm mount
172
173 2.1.1.   Dilute Crimson 1 µm carboxylate FluoSpheres beads 1:50 in PBS (2 x 10^7 beads in 1 mL
174 of PBS). If using optic bottom chambers, add Syto9 at a dilution of 1 µL to 300 µL of bead
175 preparation.
176
177 2.1.2.   (optional) Wash the biofilm to remove traces of growth medium if the growth medium
178 has autofluorescence.
179
180 2.1.2.1.   In these experiments, wash twice with 1 mL of PBS, carefully slanting the plate,
181 placing the pipette tip near the bottom edge of the well and slowly drawing out the medium.
182 Add PBS by placing the tip near the bottom edge and slowly fill the well. Use this technique
183 on optic bottom wells in addition to coverslips in a 24-well plate.
184
185 2.1.3.   Remove medium or PBS. Add diluted Crimson beads prepared in 2.1.1 to the biofilm.
186 In these studies, add 1 mL of beads ($2x10^7$) to the coverslips and 0.2 mL of beads ($4x10^6$) and
187 Syto9 to 96-well optic bottom plates.

188

189 2.1.4. Incubate for 1 min at room temperature to allow bead association.

190

191 2.1.5. Remove beads and gently wash the biofilm once with PBS to remove unassociated
192 beads. In these studies, for the coverslip, gently wash with 1 mL of PBS, refill the well with 1
193 mL PBS, and proceed to 2.1.6.

194

195 2.1.5.1. For the 96-well optic bottom plates, gently wash the biofilm with 0.2 mL of PBS
196 and refill the well with 0.2 mL of PBS. The optic bottom chamber is now ready to image, so
197 proceed to step 2.2.

198

199 2.1.6. (If using a coverslip) Add 1 µL of Syto9 (green fluorescent DNA stain; diluted per
200 manufacturer's instructions) into the center of a well on a coated 10-well multitest slide.
201 These coated coverslips have well depths of 23-25 µm.

202

203 2.1.7. (If using a coverslip) Using alcohol flame sterilized forceps, carefully remove the
204 coverslip from the well and invert onto the well containing the Syto9 drop. Leaving the
205 coverslip in 1 mL of PBS makes it easier to remove from the well and helps wash unassociated
206 beads out of the biofilm.

207

208 2.1.8. (If using a coverslip) Carefully seal the coverslip with finger-nail polish without sliding
209 or pressing down on the coverslip, which can cause surface tension that will stop movement
210 in more viscous, less rigid, biofilms.

211

212 2.1.9. (If using a coverslip) Allow the nail polish to dry. Carefully wipe the outer surface of
213 the coverslip with 70% ethanol. Wipe without apply any pressure to the coverslip for reasons
214 stated above.

215

216 2.2. Confocal imaging

217

218 NOTE: In these studies, use an inverted spectral imaging laser scanning confocal microscope
219 equipped with a TCS confocal system with the 63x objective. The scope will be used to
220 generate a 4D video (**Figure 1**). The 3D biofilm will be composed of Z slices captured in 0.5 µm
221 steps through biofilms which are 18-20 µm thick, generating 36-40 Z slices. Each 3D biofilm
222 will take 50-60 s to capture. The slices together will make up a frame, which can be visualized
223 as a 3D biofilm. This process will be repeated 20 times to generate the 4D time lapse video
224 for a total tracking time of 18-20 minutes.

225

226 2.2.1. Set the scope to capture fluorophores. In these studies, excite Syto9 (bacterial DNA
227 staining) with a 488 nm laser and measure emission from 495 to 540 nm (the Leica Sp5 is a
228 spectral imaging microscope). Excite crimson (red) beads with a 633 nm laser and measure
229 emission from 650 nm to 700 nm. These fluorophore settings can be adjusted to capture any
230 desired fluorophores.

231

232 2.2.2. Choose the xyzt imaging mode.

233

234 2.2.3. Identify a region of the biofilm with a mixture of higher and lower density regions to
235 capture differences in viscoelastic properties in thick and thin regions of the biofilm.
236
237 2.2.4. Set a Z-stack of 18-20 µm thick. In a coverslip mounted biofilm, avoid the very top and
238 very bottom of the biofilm touching against the glass to avoid bead trapping artifacts (please
239 see discussion).
240
241 2.2.5. Adjust the gain and offset to use the entire dynamic range of the intensity in the
242 brightest spot of the biofilm. This minimizes signal overlap from lower layers of the biofilm.
243
244 2.2.6. Set the slice thickness to 0.5 µm. This allows rapid imaging without the loss of bead
245 information.
246
247 2.2.7. Set resolution to 512 x 512 (0.48 µm). This allows rapid imaging yet generates images
248 with sufficient resolution to see the biofilm structure and bead movement details.
249
250 2.2.8. Minimize imaging time.
251
252 2.2.9. Set to capture 20 stacks.
253
254 2.2.10. Save as .lif (or similar confocal file). The 4D movie can be generated in ImageJ.
255
256 **3.   Generating the 4D biofilm video with ImageJ**
257
258 3.1.   Open the .lif file in ImageJ with the following settings: View stack with Hyperstack,
259 Stack order XYCZT, color mode: colorized, autoscale checked. Then press **OK**.
260
261 3.2.   Select **Image > Color > Split Channels**.
262
263 3.3.   Select **Image > Color > Merge Channels > Create Composite > OK**.
264
265 3.4.   Select **Plugins > 3D viewer > Channels uncheck blue > OK**.
266
267 3.5.   Select **Edit > Show content checked > Show bounding box checked**.
268
269 3.6.   Use the mouse click and hold to select the image. Then rotate the image while
270 continuing to hold down on the click button. Rotate the image so the bottom of the biofilm is
271 on the bottom and the angle supports visualizing the beads. Then release the image.
272
273 3.7.   Press the red **Record** button at the bottom of the window to record a video.
274
275 3.8.   Save as .avi-file using jpeg as the compression.
276
277 **4.   Generating trajectory data**
278
279 4.1.   Install the open-source tool ImageJ (https://imagej.net/Fiji) and the particle tracking
280 plugin Mosaic (https://imagej.net/MOSAICsuite).

281

282　4.2.　Import the .lif file containing the two channels for beads and bacteria. Split the
283　channels and save the files separately.

284

285　4.3.　In ImageJ, store the image voxel size (x, y, and z dimensions) and the time step size to
286　a text file.

287

288　4.4.　In ImageJ, go to **Plugins | Mosaic** and launch the Particle Tracker 2D/3D.

289

290　4.5.　Input the following parameters: Radius: 3, Cutoff: 0.003, Per/Abs: 0.12, Link Range: 2,
291　Displacement: 10.00 with the dynamics set at Brownian. Please see results for rationale
292　behind the choice of Brownian in these experiments.

293

294　4.6.　Generate trajectories and export the trajectory list as .csv files.

295

296　**5.　Analyzing trajectories**

297

298　5.1.　Install VRL Studio (https://vrl-studio.mihosoft.eu)

299

300　5.2.　Download Biofilm project (https:// neurobox3d.github.io/Biofilm/) and launch in VRL
301　Studio

302

303　5.3.　Load the trajectory file in *ImportData*

304

305　5.4.　Specify the x, y, and z pixel size (use ImageJ to locate these values) in
306　*ProcessTrajectories.*

307

308　5.5.　Specify the frame interval in *ComputeVelocity* (use ImageJ to locate this value).

309

310　5.6.　Load the bacterial tiff-file (see step 3.2) in *Comdensity.*

311

312　5.7.　Set output paths for velocity data in *SaveVelocityDataToFile* and trajectory data in
313　*SaveTrajectoryDataToFile.*

314

315　5.8.　Invoke *SaveVelocityDataToFile* and *SaveTrajectoryDataToFile.*

316

317　5.9.　Import data to Excel for analysis. These data will include trajectory lengths, trajectory
318　lifespans, trajectory bounding box dimensions and volumes, average bead velocities and
319　variances. The analysis computes weighted variables using the channel for Syto9 labelled
320　bacteria to compute the local (within given trajectory bounding boxes) cellular densities. The
321　analysis results in calculation of weighted average velocities and variances as well as weighted
322　averages and variances of bounding box variance.

323

324　**REPRESENTATIVE RESULTS:**
325　This method was used to test the hypothesis that curli may confer rigidity to *E. coli* and *S.*
326　Typhimurium biofilms, reducing bead movement during confocal microscopy experiments.
327　The current toolbox was used to compare the material properties of *Enterococcus faecalis*

328   commensal type strain OG1RF to *Salmonella enterica* serotype Typhimurium, *E. coli,* and their
329   respective isogenic curli mutants (**Figure 1B** and **Supplemental Videos 1-6**). Biofilm material
330   properties could potentially differ with respect to rigidity (e.g., curli bound to eDNA) or
331   electrostatic and hydrophobic interactions between the negatively charged beads and the
332   biofilm cells and matrix materials as well as cellular density.

333

334   *Reproducibility*
335   The Biofilm toolbox was programmed in Groovy[30] and Java[31] within VRL-Studio[32] enabling a
336   modular workflow design with automatic User Interface (UI) generation of all computational
337   components. This allowed for an automated workflow, removing unintentional
338   experimenter-induced bias when analyzing the results.

339

340   *Use of MSD to confirm type of motion in the biofilms*
341   For analysis of trajectories using Particle Tracker 2D/3D, different dynamics settings for
342   analysis of different bead movement types are available. For these studies, the setting
343   "Brownian motion" (i.e., diffusion-driven movement) was chosen since *E. faecalis* is a non-
344   motile bacterium, *E. coli* and *Salmonella* do not express flagella in biofilms, and the
345   experiments were performed in a closed system in the absence of flow. This setting could be
346   further validated by the computed mean square displacements (MSD) of the beads. Using the
347   definition $\mathrm{MSD}(m) = \frac{1}{m}\sum_{i=1}^{m}(x_i - x_0)^2$ where m is the number of trajectory segments, the
348   change of the MSD over the course of each trajectory can be computed. Linear trajectories
349   indicate diffusive bead movement (**Figure 2A**). Using quadratic least squares fitting, the
350   average movement pattern of all the beads in the biofilm was computed, showing dominant
351   linear order and validating passive diffusion as the driving force (**Figure 2A-2F**).

352

353   *Bounding box analysis.*
354   The toolbox uses ImageJ Mosaic and Particle Tracker 2D/3D to generate trajectories (Step 4)
355   and then using the automated Biofilm analysis pipeline, generates important data about the
356   bead trajectories that can be used to compare biofilm material properties. The bounding box
357   volume in μm^3 was measured by constructing the minimal box that contains a trajectory and
358   measuring its volume (**Figure 3**).

359

360   *E. faecalis* biofilms have more bead movement with bounding box values of 1-6000 μm^3
361   (**Figure 3B, 3C and 3D**). The results confirm that the movement seen in a glass coverslip
362   mounted onto a coated slide with an approximately 25 μm coated well (**Figure 3C**) versus
363   biofilms grown in the bottom of optic glass wells and directly imaged (**Figure 3D**) yield
364   equivalent results with few differences. The only difference was that near the top of the
365   mounted coverslip of *E. faecalis* biofilms stable trajectories with lifespans greater than 10
366   minutes but at the same time small bounding boxes could be registered, whereas in the optic
367   bottom plate a select number of beads with higher mobility could be registered. Taken
368   together, this suggests that mounting the glass slide may have changed the system's surface
369   tension at the top of the biofilm against the slide in the mounted coverslip biofilm, which
370   ultimately decreased mobility of some beads in less viscous biofilm regions (**Figure 3B, 3C, 3D**
371   **and 3I**). The trajectories that fall into this category happened to be a very small percentage
372   and, even with this small number of trapped beads, the average MSD of the *E. faecalis* on a
373   mounted coverslip was slightly higher than the MSD calculated from an optic bottom plate
374   biofilm (**Figure 3**).

375

376 *S.* Typhimurium and *E. coli* bead trajectories had smaller bounding box volumes of 0-10 μm^3
377 (**Figure 3A, 3B, 3E and 3F**), compared to isogenic curli mutants with bounding boxes of 1-6000
378 μm^3 for *E. coli* and 1-5000 μm^3 for *S.* Typhimurium (**Figure 3A, 3B, 3F and 3H**), demonstrating
379 larger bead mobility. These results suggested that the presence of the amyloid correlated
380 with increased rigidity in the biofilms and was consistent with the lack of notable biofilm
381 movement in the videos. The bounding box volumes were consistently small (0-10 μm^3) even
382 in low density regions of the biofilm. This observation is consistent with previous observations
383 that curli can be present in low cell density regions of the biofilm[10].

384

385 It was not possible to compare the behavior of Enterobacteriaceae biofilms on optic bottom
386 plates because they grow as pellicles on the air-liquid interface (Step 1.2.2). When using a
387 coverslip, the pellicle attached to the coverslip at the interface and when the coverslip was
388 removed the pellicle laid on the coverslip creating a single image surface. In an optic bottom
389 plate grown at a slant, imaging was done with liquid still in the well. This means the pellicle is
390 still floating above the optic bottom and makes the pellicle out of the working depth of an
391 inverted scope such as the Leica Sp5. Removing enough medium to bring the biofilm into the
392 working depth of the microscope caused the specimen to dry out over the 20-minute imaging
393 process.

394

395 Overall, the plots confirm the visual observations in the supplemental movies and are
396 consistent with the MSD differences observed (**Figure 3I and 3J**).

397

398 *Trajectory lifespans*
399 The trajectory lifespan was measured as the number of consecutive frames in which a bead
400 was registered (**Figure 3**).

401

402 In the more viscous, fluid-like *E. faecalis* biofilms, all beads had a trajectory lifespan of shorter
403 than 10 minutes and the majority of trajectories ranged between 2-5 minutes for *E. faecalis*
404 biofilms. However, beads with registered short trajectory lifespans could be located by visual
405 inspection in *E. faecalis* biofilms over the total imaging time-window (**Supplemental Video 1**
406 **and 2**). Thus, it is possible that beads move along a registered trajectory, intermittently
407 disassociating from the biofilm and terminating a trajectory, and reassociating with the
408 biofilm, at which point a new trajectory is initiated. This ultimately would lead to short
409 trajectory lifespans under continuous presence of beads in the biofilm. It is important to note
410 that using this technique, the trajectory lifespans, especially in a viscous biofilm, tends to
411 underestimate the total time a bead is associated with the biofilm.

412

413 In *S.* Typhimurium biofilms, which had smaller bounding box volumes, a majority of beads
414 (around 80%) had long trajectory lifespans of 16-20 frames, corresponding to roughly 15-20
415 minutes real-time (**Figure 3A, 3G and 3H**). Contrary to these, isogenic curli mutant biofilms
416 carried more mobile beads with bounding box volumes ranging between 1-6000 μm^3 (*E. coli*)
417 and 1-5000 μm^3 (*S.* Typhimurium) (**Figure 3A, 3B, 3F and 3H**). In contrast to *E. faecalis* biofilms
418 with >70% trajectories having bounding box volumes larger than 10 μm^3, however,
419 *Enterobacteriaceae* species biofilms registered only 30% bead trajectories with bounding box
420 volumes above 10 μm^3. Since even though overall bead trajectory lifespans were smaller in
421 curli mutant biofilms, some trajectories reflected substantial bead movement and long

422 trajectory lifespans (**Figure 3H**). This observation could indicate that this variability may
423 correspond to varying biofilm material properties, such as viscoelasticity, and/or particle
424 surface chemistry changes such as charge.
425
426 *Analysis of bead trajectory lengths and velocities*
427 The trajectory length is a measurement of the distance traveled by beads in μm. This
428 measurement is consistent with the velocity of bead movement in μm/s. Consistent with the
429 larger bounding box volumes, beads in *E. faecalis* biofilms had 10-fold longer trajectories, 5-
430 20 μm, versus <4 μm in biofilms containing curli. Consistent with the shorter trajectories
431 (**Figure 4A**). *E. faecalis* beads measured up to 15x higher velocities with a majority of beads
432 having velocities in the range of 0.01-0.15 μm/s versus velocities <0.006 μm/s (**Figure 4B**).
433 Nonetheless, curli mutant biofilms measured overall lower velocities and shorter trajectories
434 compared to *E. faecalis* biofilms, but longer trajectories and higher velocities than the curli
435 containing parental strains (**Figure 4A and 4B**).
436
437 Noteworthy is the fact that the fibrillar lattice-like structure of curli[30] may affect mobility in
438 an anisotropic way, reducing movement in the xy-plane and allowing increased mobility in
439 the z-direction (**Figure 2G**). The large trajectory pool (approximately 800) belonging to roughly
440 50 unique beads in curli-containing biofilms would be consistent with the limitations of
441 Mosaic Particle Tracking, counting each one of these rapidly moving beads as a single bead in
442 x, y and z. Additional research and software development will be necessary to confirm this
443 observation.
444
445 *Analysis of bead movement dependence on cellular density*
446 The dependence of bead movement on cellular density was determined by using weighted
447 average velocities and variances, as well as averages/weighted averages and variances of
448 bounding box volumes. The second imaging channel for Syto9 labelled bacteria was used to
449 compute the local cellular densities in the calculation of weighted velocities. The cellular
450 density was computed by averaging the Syto9 voxel data over the bounding box of each
451 trajectory edge (**Figure 5**, right). Thus, the bead velocity can be weighted by the edge-wise
452 (local) cell densities. There are multiple types of stains that could be used to visualize bacteria
453 including stains for the cell wall, membranes, and DNA content. To determine cellular density
454 Syto9 was chosen because it gives the most consistent signal no matter which optical Z slice
455 is being visualized. Envelope stains (cell wall and membrane) will give a different signal
456 depending on the position of the Z slice. If the Z slice includes the top or bottom of the cell,
457 the signal will be stronger than if the Z slice is through the middle of the cell where only the
458 outline of the cell is stained.
459
460 The bead trajectories from the red channel were tracked for 20 frames, where individual
461 trajectories had a minimal lifespan of 2 frames and a maximum of 20 frames with 19 trajectory
462 segments connecting the frames (**Figure 5**). To study cell density dependence of bead
463 mobility, the GFP intensity per voxel (each of the individual measurements in the 512x512
464 voxel image) was determined. The cell density around each segment of the bead trajectory
465 was calculated as the locally averaged density in the bounding box of the segment.
466
467 For some biofilms, statistically significant density-dependence could be documented (**Figure**
468 **6**), most prominently for *E. faecalis* biofilms that were grown on a glass coverslip and inverted

469 onto a multiwell slide (**Figure 6C**). To the contrary, *E. faecalis* biofilms that were grown on the
470 bottom of a 96 well plate (**Figure 6D**) showed no density dependence. In conclusion, this
471 suggests that highly fluid *E. faecalis* biofilms could potentially be slightly compressed due to
472 the mounting on a multi-well slide, which is consistent with a reduction in the number of
473 beads moving more rapidly and those with small bounding box volumes that are trapped at
474 the top of the biofilm against the glass slide (**Figure 3C** vs **Figure 3D**). Both the *Salmonella* and
475 *E. coli* biofilms (**Figure 6C and 6D**) and their isogenic mutants (**Figure 6E and 6F**) showed minor
476 to no cellular density dependence.

478 **FIGURE AND TABLE LEGENDS:**

480 **Figure 1. Imaging and analysis pipeline (steps 2-4) (A)** Biofilms are imaged as outlined in 2.2.
481 Using the imaged biofilms (see 3) bead trajectories were generated as described in 4. Using
482 the trajectories relevant data was computed with the analysis toolbox (see 5) (**B**) Biofilms
483 were grown as described in step 1 on coverslips (*E. faecalis,* **Video 1**), *S.* Typhimurium (**Video**
484 **3**), *E. coli* (**Video 5**) and isogenic curli mutants (**Video 4, Video 6**) or in an optic bottom 96-
485 well plate (*E. faecalis* bottom, **Video 2**). The white scale bar is 20 mm. This figure is reproduced
486 with permission from (31).

488 **Figure 2. The bead movement in the biofilms were determined to be diffusive in nature**
489 **(Brownian motion, see step 5) (A-F)** MSD data shows linear behavior (red line) to validate
490 Brownian motion. Biofilms were grown according to step 1 (**G**) Example of elliptical bead
491 movement observed in *E. coli* and *S.* Typhimurium biofilms taken from one frame of the *E.*
492 *coli* 4D biofilm assay (**H**) Example of large changes in bead patterns between frame 3 and 4
493 taken from *E. faecalis* optic bottom well. Note the biofilm itself elicits some flow (**Video 1 and**
494 **2**), which makes it appear that frame 3 and 4 are differently oriented. This figure is reproduced
495 with permission from (31).

497 **Figure 3. Analysis of differences in rigidity using bounding boxes and trajectory lifespans.**
498 Biofilms were grown as described in step 1 on coverslips (*E. faecalis,* **Video 1**), *S.* Typhimurium
499 (**Video 3**), *E. coli* (**Video 5**) and isogenic curli mutants (**Video 4, Video 6**) or in an optic bottom
500 96-well plate (*E. faecalis* bottom, **Video 2**). Trajectory lifespans are presented in % of total
501 bead trajectories (**A**) and scatter graphs (**C-H**), along with bounding box volumes (computed
502 in step 5) (**I**) Comparison of the bead MSDs in the different biofilms (**H**) Average MSDs of each
503 type of biofilm. The bars indicate the 95% confidence interval of the data. This figure is
504 reproduced with permission from (31).

506 **Figure 4. Analysis of differences in trajectory length and bead velocity.** Biofilms were grown
507 as described in step 1. Trajectory lengths are shown in μm and are presented as % of total
508 bead trajectories (**A**). Velocity is shown in μm/s and presented as % of total bead trajectories
509 (**B**). This figure is adapted with permission from (31).

511 **Figure 5. Outline of trajectory segment analysis.** This figure is adapted with permission from
512 (31).

514 **Figure 6. Studying the effect of biofilm density on bead velocity using the biofilm analysis**
515 **pipeline (step 5).** Results indicated that bead velocity is not exclusively cell density

516 dependent. Biofilms were grown as described in step 1. Trajectories were analyzed at the
517 scale of individual trajectory segments (Figure 5). For each segment, bead velocity in μm/s
518 was plotted against bounding box cellular density (average GFP per voxel within the bounding
519 box). The red line shows the linear regression, and the green line the exponential regression
520 trace. This figure is reproduced with permission from (31).
521
522 **Supplemental Figure 1. 4D video of 24-hour *E. faecalis* OG1RF biofilm grown on a 1.5 thick**
523 **optic glass coverslip.** The 4D time lapse video was generated using a microscope at 512x512
524 resolution. A Z-series of 40 images was generated by imaging an approximately 20 μm thick
525 region of a biofilm in 0.5 μm steps. Each Z series was one frame and required 50-60 s to
526 capture. A series of 20 contiguous frames were captured to produce a 4D video. The video
527 playback is at approximately 120x. Video is representative of at least 6 independent
528 experiments.
529
530 **Supplemental Figure 2. 4D video of a 24-hour *E. faecalis* OG1RF biofilm grown on a 96-well**
531 **optic bottom plate.** The 4D time lapse video was generated using a microscope at 512x512
532 resolution. A Z-series of 40 images was generated by imaging an approximately 20 μm thick
533 region of a biofilm in 0.5 μm steps. Each Z series was one frame and required 50-60 s to
534 capture. A series of 20 contiguous frames were captured to produce a 4D video. The video
535 playback is at approximately 120X.Video is representative of 3 independent experiments.
536
537 **Supplemental Figure 3. 4D video of a *Salmonella enterica* serotype Typhimurium biofilm**
538 **ATCC 14028 grown on 1.5 thick optic glass coverslips for 6-7 days.** The 4D time lapse video
539 was generated using a microscope at 512x512 resolution. A Z-series of 40 images was
540 generated by imaging an approximately 20 μm thick region of a biofilm in 0.5 μm steps. Each
541 Z series was one frame and required 50-60 s to capture. A series of 20 contiguous frames were
542 captured to produce a 4D video. The video playback is at approximately 120x. Video is
543 representative of 3 independent experiments.
544
545 **Supplemental Figure 4. 4D video of *Salmonella enterica* serotype Typhimurium biofilms**
546 **ATCC 14028 curli (*csgBA*) mutant were grown on 1.5 thick optic glass coverslips for 6-7 days.**
547 The 4D time lapse video was generated using a microscope at 512x512 resolution. A Z-series
548 of 40 images was generated by imaging an approximately 20 μm thick region of a biofilm in
549 0.5 μm steps. Each Z series was one frame and required 50-60 s to capture. A series of 20
550 contiguous frames were captured to produce a 4D video. The video playback is at
551 approximately 120x. Video is representative of 3 independent experiments.
552
553 **Supplemental Figure 5. 4D video of *E. coli* UTI89 grown on 1.5 thick optic glass coverslips**
554 **for 6-7 days.** The 4D time lapse video was generated using a microscope at 512x512
555 resolution. A Z-series of 40 images was generated by imaging an approximately 20 μm thick
556 region of a biofilm in 0.5 μm steps. Each Z series was one frame and required 50-60 s to
557 capture. A series of 20 contiguous frames were captured to produce a 4D video. The video
558 playback is at approximately 120x. Video is representative of 3 independent experiments.
559
560 **Supplemental Figure 6. 4D video *E. coli* UTI89 curli (*csgBA*) mutant grown on 1.5 thick optic**
561 **glass coverslips for 6-7 days.** The 4D time lapse video was generated using a microscope at
562 512x512 resolution. A Z-series of 40 images was generated by imaging an approximately 20

563   μm thick region of a biofilm in 0.5 μm steps. Each Z series was one frame and required 50-60
564   s to capture. A series of 20 contiguous frames were captured to produce a 4D video. The video
565   playback is at approximately 120x. Video is representative of 3 independent experiments.
566
567   **DISCUSSION:**
568   **Critical steps and troubleshooting**
569   The biggest challenge of this technique is using a mounted coverslip with a very viscous
570   biofilm like *E. faecalis.* The coverslip needs to be carefully and accurately placed on the
571   multiwell slide without repositioning it. During the sealing step, care needs to be used to
572   prevent pushing down on the coverslip or accidently pushing/sliding it across the slide
573   surface. Any movement or pressure may create surface tension and block movement of a
574   viscous biofilm. If possible, comparing biofilm material properties by imaging a biofilm on an
575   optic bottom well to a coverslip mount will allow technique assessment. When correctly
576   performed, a coverslip mount very closely resembled a biofilm in an optic bottom plate for *E.*
577   *faecalis*.
578
579   In addition, when using a mounted coverslip, imaging of the interfaces of the biofilm with the
580   coverslip at the bottom or the slide at the very top should be avoided. When using an inverted
581   scope, with the coverslip at the bottom, there can be trapped beads at the base of the biofilm
582   against the coverslip. These beads pass through the biofilm and become trapped against the
583   coverslip even after gentle washing. They have x, y and z coordinates of 0 and bounding box
584   coordinates of 0. However, for certain applications, such as examining biofilm integrity after
585   treatment, these data points can be used as a tool. The ability of beads to penetrate through
586   a thick region of biofilm to the bottom of coverslip can be used to assess biofilm integrity after
587   treatment (manuscript in preparation in collaboration with Tükel laboratory). At the top of
588   the biofilm, in a viscous biofilm like *E. faecalis* we had some evidence of compaction imposed
589   by the coverslip. This limited the movement of some beads at the glass slide interface and
590   may have introduced some density dependence to the bead movement analysis.
591
592   The washing steps were necessary for the biofilms because he growth medium has strong
593   autofluorescence in the green channel. We choose to use excess beads and remove
594   unassociated beads by washing to maximize the associated beads to get the most accurate
595   characterization of the observed regions.
596
597   The number of beads and washes needed to obtain desired data sets needs to be determined
598   empirically. The presence of too many beads in a biofilm generates impossibly large data sets
599   that are hard to analyze. The presence of too few beads does not generate a thorough
600   sampling of the biofilm environments. However, control of the number of beads added (2×10^7
601   beads in 1 mL of PBS) and the use of wash steps, resulted in a relatively consistent number of
602   beads (40-140) associating with the biofilm depending on its structure, spatial arrangement,
603   and composition.
604
605   When studying biofilms with mixed viscous and rigid regions, beads can become trapped in
606   the rigid regions over time. In this case, imaging needs to be started immediately after
607   addition of the beads. This often cannot be accomplished using coverslips but requires optic
608   bottom plates or flow cells where imaging can be done immediately after addition of the
609   beads and the wash step(s).

610
611 **Modifications and Future Applications**
612 *Use of microfluidic devices.* In our studies, the optimal conditions established for the study of
613 the Enterobacteriaceae biofilms required growth of the biofilm as a pellicle at the air-liquid
614 interface. This limited the use of optic bottom plates and microfluidic devices in the studies.
615 However, when biofilm formation conditions permit, the biofilms can be grown in microfluidic
616 chambers or flow cells. The biofilms could then be washed, and beads introduced through the
617 microfluidic device with minimal disruption of the biofilm.
618
619 *Addition of beads during biofilm growth.* We chose to add excess beads to the biofilms, and
620 then remove unassociated beads by gentle washing to optimize the number of beads present
621 during the analysis. In the viscous *E. faecalis* biofilms, it is possible that the beads
622 disassociated and reassociated with during the 20-minute imaging time. If a low number of
623 beads are added at different times during biofilm growth, it might be possible to trap the
624 beads in the biofilm, allowing more accurate characterization of the biofilm movement in
625 more viscous biofilms.
626
627 *Choice of the region to image*. For studies on material properties, it is best to choose thick
628 and thin regions of the biofilm. However, when studying changes in the material properties
629 of a treated biofilm, thick confluent regions may be imaged to determine changes in
630 viscoelastic properties and bead penetration in those regions. In this case, looking for beads
631 that penetrated the biofilm and ended up trapped against the coverslip are a useful measure
632 of biofilm disruption.
633
634 *Imaging under flow*. Using optic glass flow cells or microfluidic devices, movement of beads
635 or bacteria in a biofilm under flow can be imaged. This can be done in different ways. It can
636 be done by injection of beads into the whole chamber followed by brief incubation to allow
637 association of the beads with the biofilm. The unassociated beads can be removed by washing
638 and the biofilm imaged with or without flow. Conversely, a small number of beads can be
639 introduced into one side of the chamber and their movement through and in the biofilm can
640 be tracked under flow. When using flow, caution will need to be used in choosing the Mosaic
641 bead tracking settings (Step 4.5). In the current studies the dynamics setting was Brownian.
642 MSD calculations confirmed that the movement was likely to be diffusive, making Brownian
643 the appropriate setting.
644
645 *Matrix staining*. In the current studies, staining with Syto9 examines cellular density and not
646 biofilm structure density. For example, the presence of amyloids likely increases the density
647 of the matrix material of the biofilm. The dependence of movement on the amyloid density
648 could be determined by using fluorescent matrix stains in lieu of Syto9.
649
650 *Fluorescently labelled bacteria.* Fluorescently labelled bacteria can be used to track
651 movement of exogenous bacteria through biofilms (*e.g.*, plasmid-containing bacteria). The
652 challenge with fluorescently labelled bacteria, such as *Enterococci,* is that they form singles,
653 diplococci, and short chains, which complicates the ability to accurately track the bacteria.
654 This process would be easier if the bacteria have a single-cell morphology.
655
656 **Limitations**

657 *Limitations in trajectory visualization and stitching.*
658 One limitation of the method is trajectory visualization and stitching. Reconstructed and
659 analyzed trajectories consist of x, y, z point coordinates, where subsequent points define the
660 linear path between these points. Visualization of such piecewise linear trajectories can be
661 achieved by various tools. One approach was to use Python and Jupyter notebooks together
662 with the Python plugins, Pandas and Matplotlib. While it was possible to visualize individual
663 existing trajectories in the Journal of Bacteriology article where this technique was originally
664 published[34], there were still significant limitations that are being addressed in future research.
665
666 Currently, the number of reconstructed trajectories is larger than the number of beads in the
667 biofilm, meaning multiple trajectories may correspond to one bead. This can be caused by a
668 weak confocal signal in one frame where Mosaic will terminate a trajectory and initiate a
669 second. This may register as multiple shorter trajectories for one bead, especially in less
670 viscous biofilms. Another cause for the large number of trajectories is the lack of trajectory
671 stitching. Especially in *E. faecalis* optic bottom well biofilms, beads visually remain associated
672 with the biofilm during imaging (**Supplemental Video 2**). However, there were no trajectories
673 longer than 10 and over 90% of the trajectories had a lifespan of 5 frames or less (**Figure 3D**).
674 If the software is used to analyze only trajectories above a defined length (e.g., when tracing
675 cells that are capable of transferring plasmids), shorter trajectories can automatically be
676 removed from the data set. However, there are other purposes for which stitching the
677 trajectories may be very important. Finally, the inability to track rapid bead movement as a
678 single trajectory could result in more trajectories in Enterobacteriaceae biofilms due to the
679 rapid movement in the Z direction resulting in elliptical-shaped beads (**Figure 2G**). The
680 possibility of stitching trajectories disrupted by rapid anisotropic movement will be important
681 to study the effect of the curli amyloid matrix in Enterobacteriaceae.
682
683 **Significance**
684 A computational workflow was developed to study bead trajectories to compare the material
685 properties of 3D biofilms. The workflow enables researchers to identify critical parameters
686 that can be used in computational modeling of fluid dynamics in heterogeneous biofilms.
687 With the help of this open-source bead evaluator, the effect bacterial amyloid curli on the
688 material properties could be studied, showing increased biofilm matrix rigidity due to curli. In
689 a more general context, the evaluator can be used to study changes in biofilm structure
690 induced by biofilm treatment or different environmental conditions, such as flow. For
691 example, the tool is being used to analyze the effect of monoclonal antibody treatment on
692 the disruption of biofilm structures in collaboration with the Tükel laboratory (LKSOM Temple
693 University). The bead evaluator toolbox is fully adaptable and extendable in a modular fashion
694 using VRL-Studio to further enhance and extend its functions.
695

702
703 **DISCLOSURES:**

The authors have nothing to disclose.

REFERENCES:
1.   Huang, R., Li, M., Gregory, R.L. Bacterial interactions in dental biofilm. *Virulence*. **2**, 435–444 (2011).
2.   Nadell, C.D., Drescher, K., Wingreen, N.S., Bassler, B.L. Extracellular matrix structure governs invasion resistance in bacterial biofilms. *ISME Journal*. **9**, 1700–1709 (2015).
3.   Billings, N., Birjiniuk, A., Samad, T.S., Doyle, P.S., Ribbeck, K. Material properties of biofilms – key methods for understanding permeability and mechanics. *Reports on Progress in Physics*. **78**, 036601 (2015).
4.   Araújo, G.R. de S., Viana, N.B., Gómez, F., Pontes, B., Frases, S. The mechanical properties of microbial surfaces and biofilms. *The Cell Surface*. **5**, 100028 (2019).
5.   Tallawi, M., Opitz, M., Lieleg, O. Modulation of the mechanical properties of bacterial biofilms in response to environmental challenges. *Biomaterials Science*. **5**, 887–900 (2017).
6.   Tursi, S.A., Tükel, Ç. Curli-Containing Enteric Biofilms Inside and Out, Matrix Composition, Immune Recognition, and Disease Implications. *Microbiology and Molecular Biology Reviews*. **82** (2018).
7.   Dueholm, M.S., Albertsen, M., Otzen, D., Nielsen, P.H. Curli functional amyloid systems are phylogenetically widespread and display large diversity in operon and protein structure. *PLoS One*. **7** (12), e51274 (2012).
8.   Hung, C. et al. *Escherichia coli* biofilms have an organized and complex extracellular matrix structure. *mBio*. **4**, e00645-00613 (2013).
9.   Kikuchi, T., Mizunoe, Y., Takade, A., Naito, S., Yoshida, S. Curli fibers are required for development of biofilm architecture in *Escherichia coli* K-12 and enhance bacterial adherence to human uroepithelial cells. *Microbiology and Immunology*. **49**, 875–884 (2005).
10.   Gallo, P.M. et al. Amyloid-DNA Composites of Bacterial Biofilms Stimulate Autoimmunity. *Immunity*. **42**, 1171–1184 (2015).
11.   Serra, D.O., Richter, A.M., Hengge, R. Cellulose as an architectural element in spatially structured *Escherichia coli* biofilms. *Journal of Bacteriology*. **195**, 5540–5554 (2013).
12.   Oh, Y.J. et al. Characterization of curli A production on living bacterial surfaces by scanning probe microscopy. *Biophysical Journal*. **103**, 1666–1671 (2012).
13.   Lembré, P., Di Martino, P., Vendrely, C. Amyloid peptides derived from CsgA and FapC modify the viscoelastic properties of biofilm model matrices. *Biofouling*. **30**, 415–426 (2014).
14.   Oh, Y.J. et al. Curli mediate bacterial adhesion to fibronectin via tensile multiple bonds. *Scientific Reports*. **6**, 33909 (2016).
15.   Vidakovic, L., Singh, P.K., Hartmann, R., Nadell, C.D., Drescher, K. Dynamic biofilm architecture confers individual and collective mechanisms of viral protection. *Nature Microbiology*. **3**, 26–31 (2018).
16.   Tursi, S.A. et al. *Salmonella* Typhimurium biofilm disruption by a human antibody that binds a pan-amyloid epitope on curli. *Nature Communications*. **11**, 1007 (2020).
17.   Perov, S. et al. Structural Insights into Curli CsgA Cross-β Fibril Architecture Inspire Repurposing of Anti-amyloid Compounds as Anti-biofilm Agents. PLOS Pathogens. **15** (8), e1007978 (2019).
18.   Taglialegna, A. et al. The biofilm-associated surface protein Esp of Enterococcus faecalis forms amyloid-like fibers. *Npj Biofilms and Microbiomes*. **6**, 15 (2020).

19.   Gour, S., Kumar, V., Rana, M., Yadav, J.K. Pheromone peptide cOB1 from native *Enterococcus faecalis* forms amyloid-like structures, A new paradigm for peptide pheromones. *Journal of Peptide Science*. **25**, e3178 (2019).

20.   Stoodley, P., Debeer, D., Lewandowski, Z. Liquid flow in biofilm systems. *Applied and Environmental Microbiology*. **60**, 2711–2716 (1994).

21.   Birjiniuk, A. et al. Single particle tracking reveals spatial and dynamic organization of the *E. coli* biofilm matrix. *New Journal of Physics*. **16**, 085014 (2014).

22.   Chew, S.C. et al. Dynamic remodeling of microbial biofilms by functionally distinct exopolysaccharides. *mBio*. **5**, e01536-01514 (2014).

23.   Cao, H. et al. Revealing region-specific biofilm viscoelastic properties by means of a micro-rheological approach. *Npj Biofilms and Microbiomes*. **2**, 5 (2016).

24.   Galy, O. et al. Mapping of bacterial biofilm local mechanics by magnetic microparticle actuation. *Biophysical Journal*. **103**, 1400–1408 (2012).

25.   Rogers, S.S., van der Walle, C., Waigh, T.A. Microrheology of bacterial biofilms in vitro, *Staphylococcus aureus* and *Pseudomonas aeruginosa*. *Langmuir*. **24**, 13549–13555 (2008).

26.   Hart, J.W., Waigh, T.A., Lu, J.R., Roberts, I.S. Microrheology and Spatial Heterogeneity of Staphylococcus aureus Biofilms Modulated by Hydrodynamic Shear and Biofilm-Degrading Enzymes. *Langmuir*. **35** (9), 3553-3561 (2019).

27.   van Merode, A.E.J., van der Mei, H.C., Busscher. H.J., Krom, B.P. Influence of culture heterogeneity in cell surface charge on adhesion and biofilm formation by *Enterococcus faecalis. Journal of Bacteriology*. **188**, 2421–2426 (2006).

28.   Tariq, M., Bruijs, C., Kok, J., Krom, B.P. Link between Culture Zeta Potential Homogeneity and Ebp in *Enterococcus faecalis*. *Applied and Environmental Microbiology*. **78**, 2282–2288 (2012).

29.   Schneider, C.A., Rasband, W.S., Eliceiri, K.W. NIH Image to ImageJ, 25 years of image analysis. *Nature Methods*. **9**, 671–675 (2012).

30.   http, //groovy-lang.org (2021).

31.   https, //docs.oracle.com/en/java (2021).

32.   Hoffer, M., Poliwoda, C., Wittum, G. Visual reflection library, a framework for declarative GUI programming on the Java platform. *Computing and Visualization in Science*. **16**, 181–192 (2013).

33.   Perov, S. et al. Structural Insights into Curli CsgA Cross-β Fibril Architecture Inspire Repurposing of Anti-amyloid Compounds as Anti-biofilm Agents. *PLOS Pathogens*. **15**, e1007978 (2019).
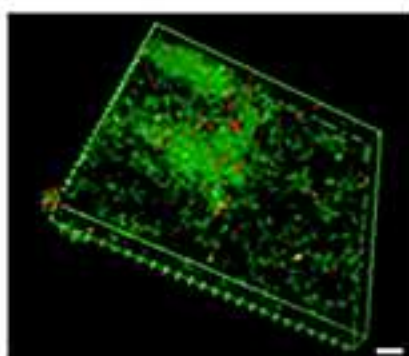
34.   Malhotra, K. et al. Development of a New Bead Movement-Based Computational Framework Shows that Bacterial Amyloid Curli Reduces Bead Mobility in Biofilms. *Journal of Bacteriology.* **202**, e00253-20 (2020).
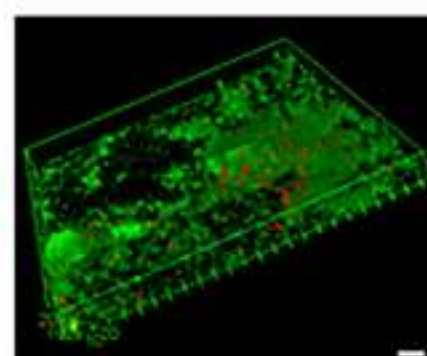
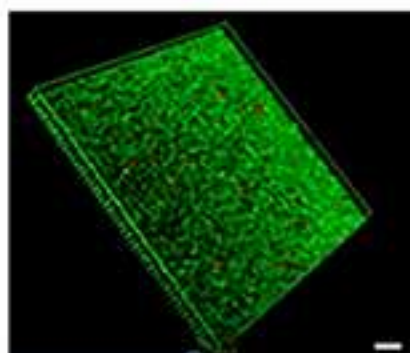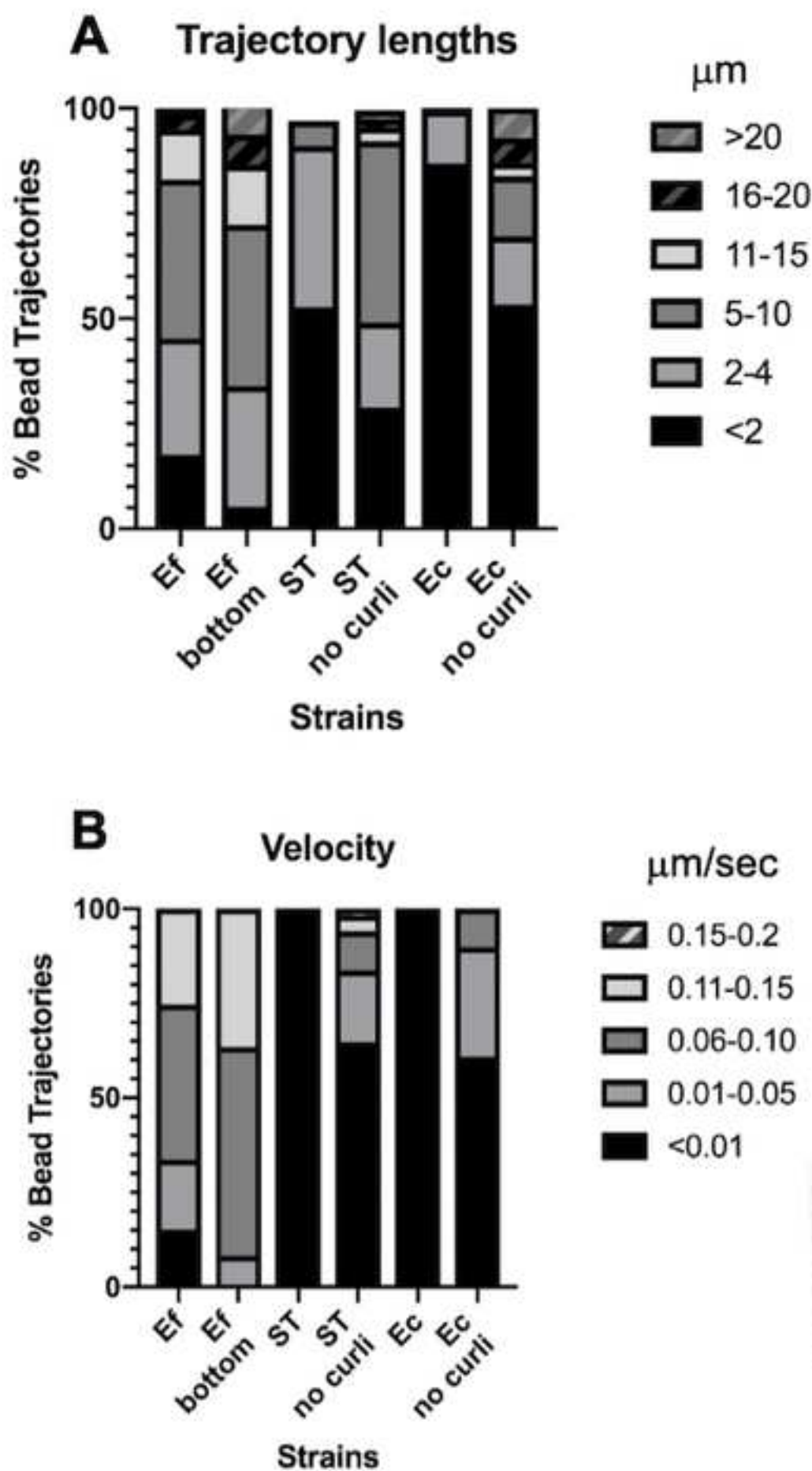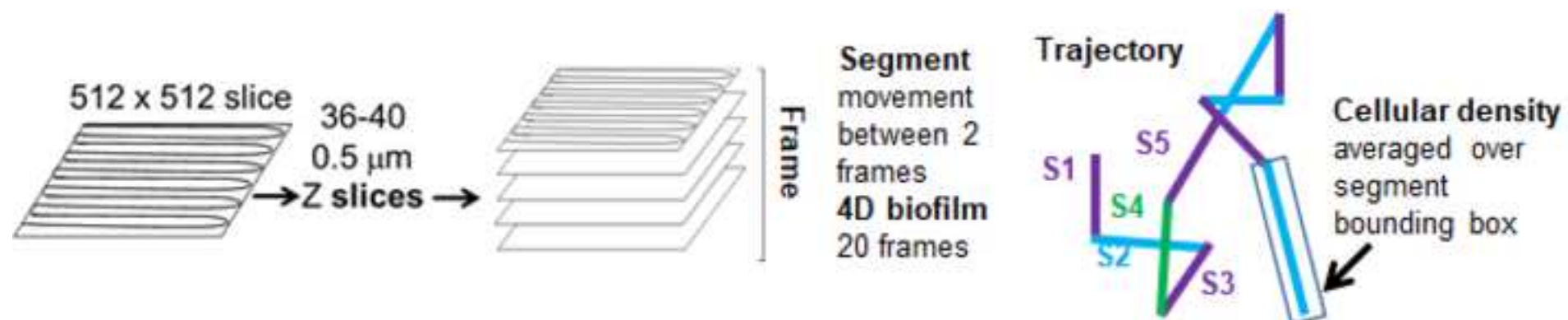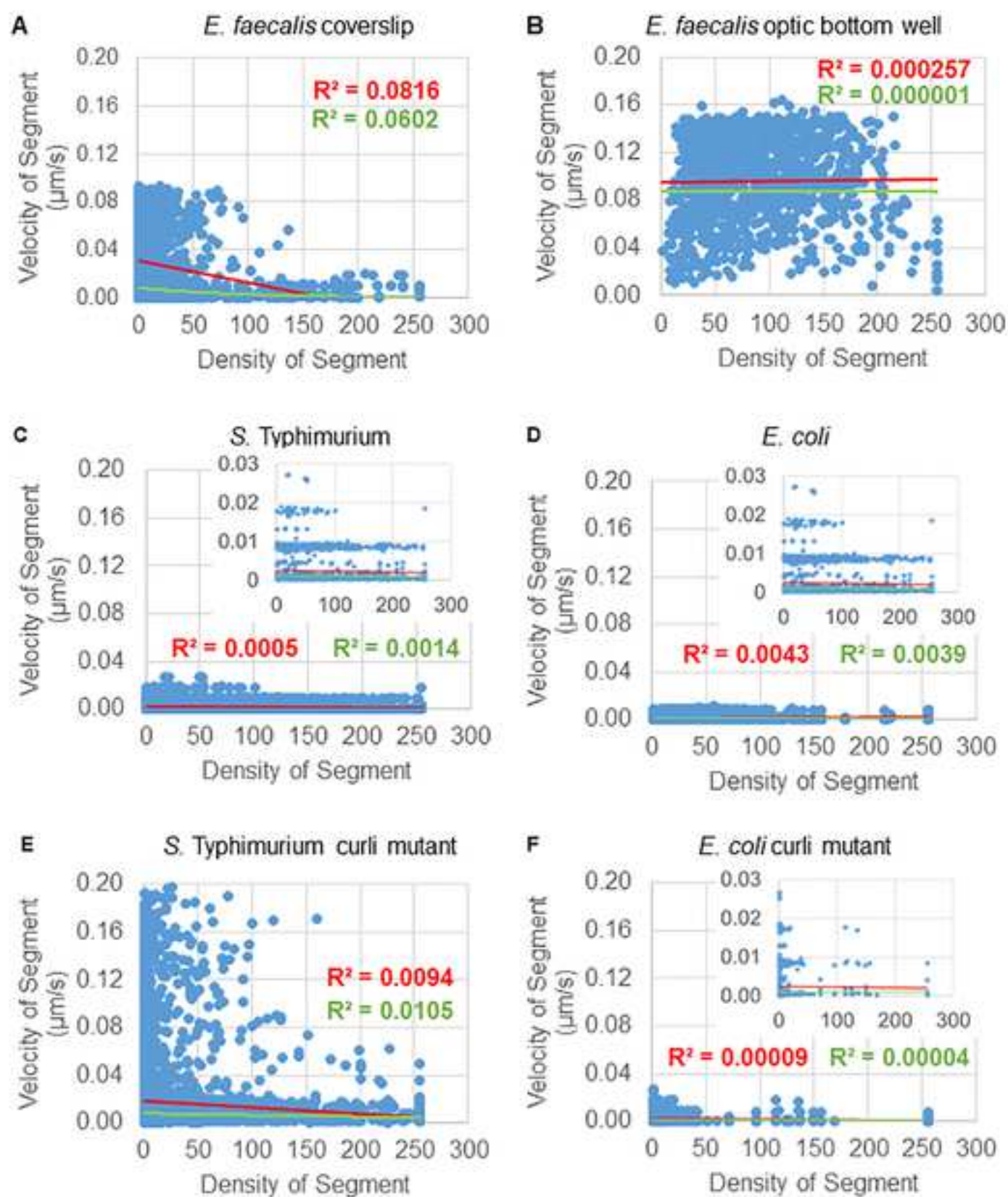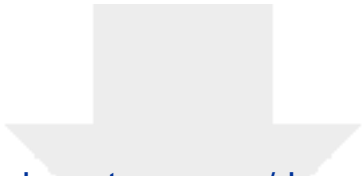Figure 1   Click here to access/download;Figure;Fig 1.tif ⬇
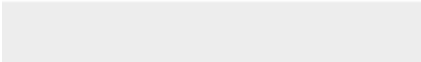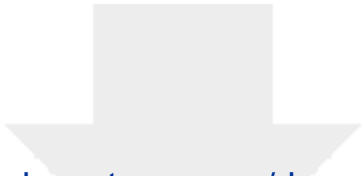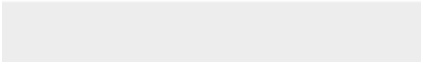

A 512 x 512 slice 36-40 0.5 μm →Z slices→ = frame approx. 50-60s 20 X frames → 4D time lapse movie → 3D biofilm

Toolbox → trajectory and visualization → bounding box (μm³) velocity (μm/sec) → trajectory lifespan (frames) trajectory length mean square displacement
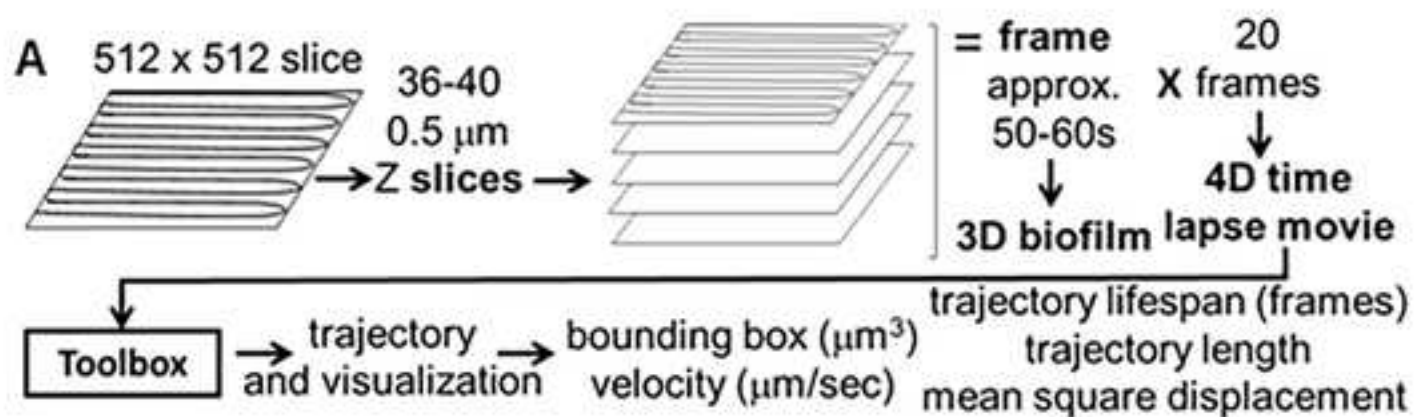
B *E. faecalis* coverslip Video 1
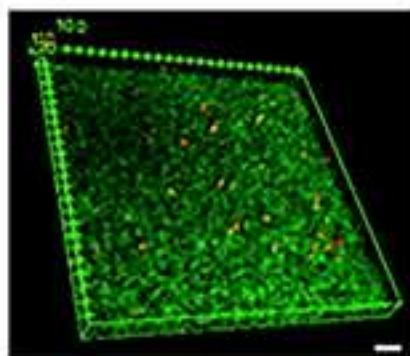
S. Typhimurium Video 3

E. coli Video 5

E. faecalis optic bottom Video 2

S. Typhimurium curli mutant Video 4
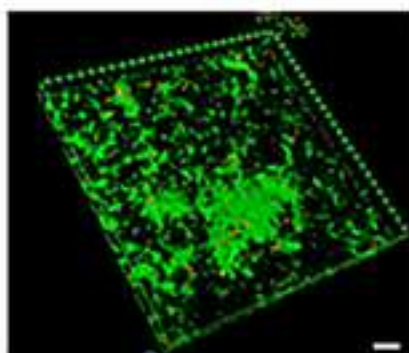
E. coli curli mutant Video 6
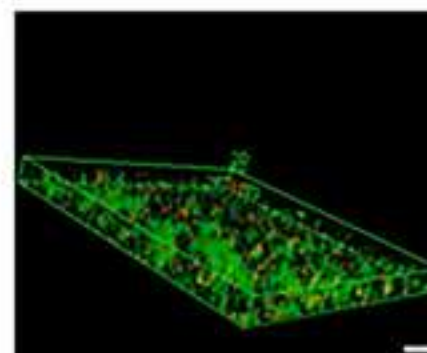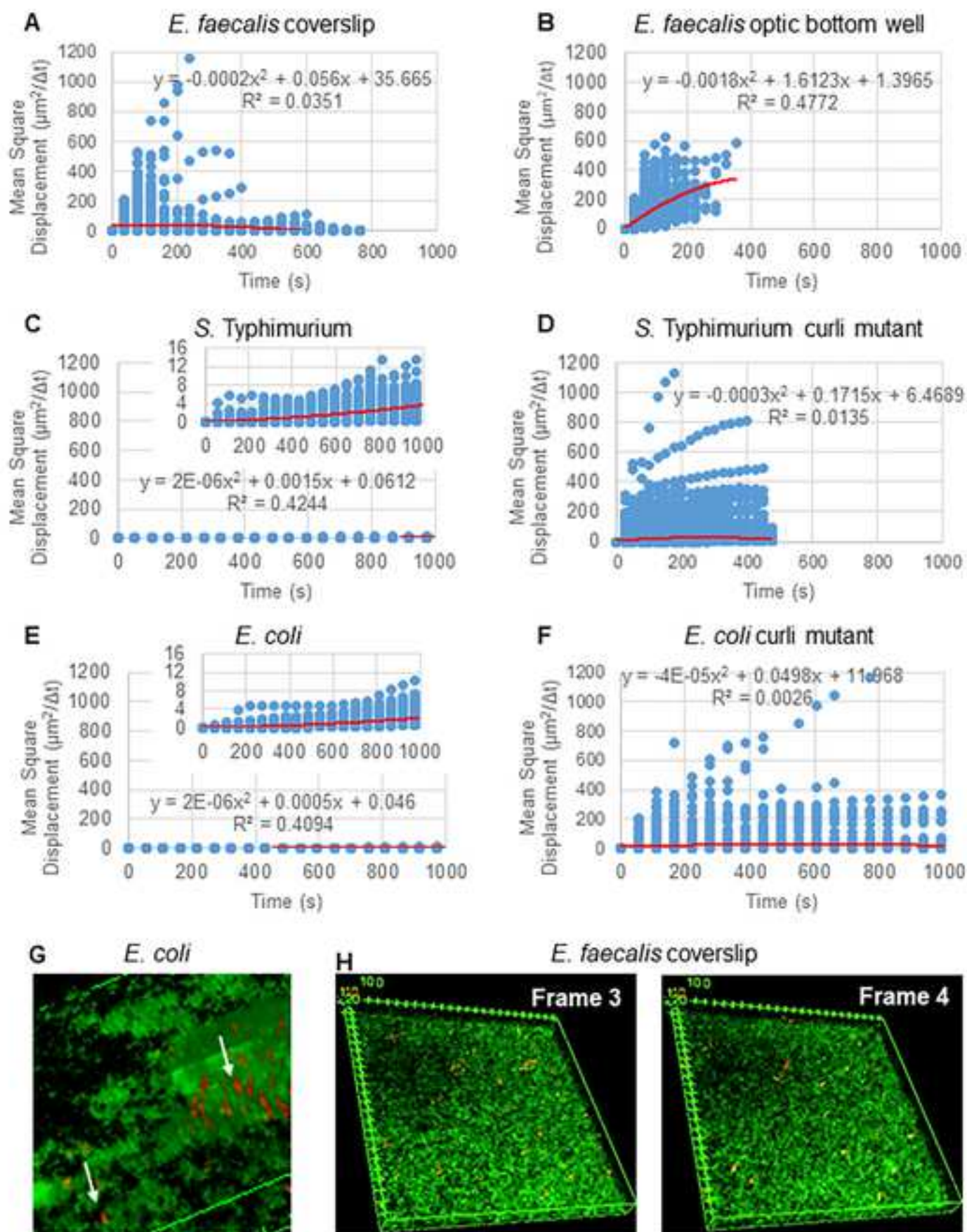
Figure 2　　　　　　　　　　　　　　　　　　　　　　　　　Click here to access/download;Figure;Fig 2.tif ⬇

Figure 3

Figure 4

A Trajectory lengths

μm
- >20
- 16-20
- 11-15
- 5-10
- 2-4
- <2

B Velocity

μm/sec
- 0.15-0.2
- 0.11-0.15
- 0.06-0.10
- 0.01-0.05
- <0.01

Figure 5   Click here to access/download;Figure;Fig 5.tif ⬇

512 x 512 slice

36-40
0.5 μm
→Z slices →

Frame

Segment
movement
between 2
frames
4D biofilm
20 frames

Trajectory

S1   S5

S4

S2   S3

Cellular density
averaged over
segment
bounding box

Figure 6

Figure 6

Supplemental Video 1
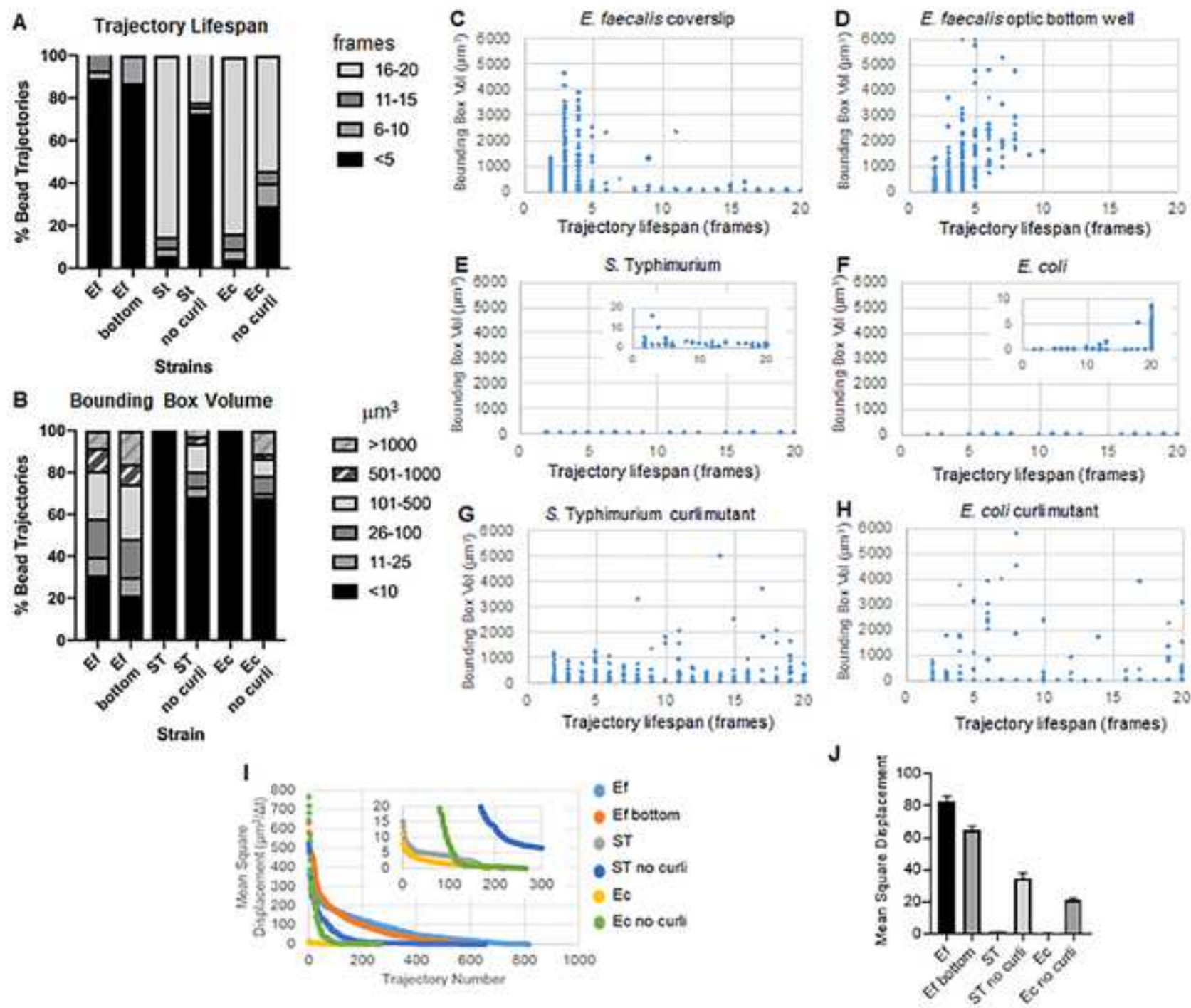
Click here to access/download
Video or Animated Figure
S1 faecalis.avi

Click here to access/download
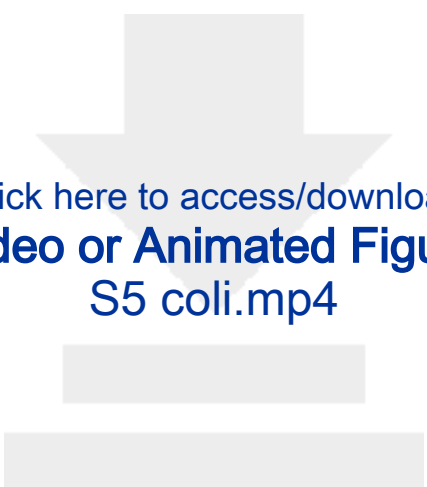**Video or Animated Figure**
S2 faecalis bottom.avi

Click here to access/download
Video or Animated Figure
S3 Salmonella.avi

Click here to access/download
Video or Animated Figure
S4 Salmonella no curli.avi

Click here to access/download
Video or Animated Figure
S5 coli.mp4

Click here to access/download
Video or Animated Figure
S6 coli no curli.mp4

Name of Material/Equipment	Company	Catalog Number	Comments/Description
96-well plates, No. 1.5 Uncoated Coverslip, 5 mm Glass Diameter	MatTek	P96G1.55F	
Fisherbrand Cover Glasses: Circles	Fisher Scientific	12-293-232P	1.5 optic glass coverslip
Invitrogen Syto 9 Green Fluorescent Nucleic Acid Stain	Invitrogen	S34854	
Molecular Probes FluoSpheres Carboxylate-modified Microspheres, 1 um, crimson fluorescent (625/645)	Molecular Probes	F8816	

TEMPLE
UNIVERSITY

Bettina A. Buttaro, Ph.D.
Department of Microbiology and Immunology
3400 N. Broad St.
Philadelphia, PA 19140
+1.215.707.3212
bbuttaro@temple.edu

Lewis Katz School of Medicine

May 4, 2021

Dear Dr. Nguyen,

This letter accompanies the revised version of our manuscript "Bead movement based computational framework for 3-dimensional analysis of biofilm material heterogeneity" by B. Buttaro and G. Queisser. Following this cover letter, is a point-by-point response to the reviewers. The reviewer's comments are in black. Our responses to the reviewers are in blue in the response letter and the manuscript.

We could not address one issue raised about the quality of the images. The images are the ones used in the Journal of Bacteriology article, so they should be of significant quality. Perhaps it was a problem with the assembled pdf? We are happy to work with you to meet the quality requirements.

We hope these changes will make the manuscript suitable for publication.

Bettina A Buttaro

Bettina A. Buttaro, Ph.D.
Assoc. Prof. Microbiol. Immunol.

[signature]

Gillian Queisser, Ph.D.
Assoc. Prof. Mathematics

Editorial comments:
Changes to be made by the Author(s) regarding the written manuscript:
1. Please take this opportunity to thoroughly proofread the manuscript to ensure that there are no spelling or grammar issues. We hope we have not missed any errors.
2. Please provide emails and affiliations for both authors. Affiliations were added.
3. JoVE cannot publish manuscripts containing commercial language. This includes trademark symbols (™), registered symbols (®), and company names before an instrument or reagent. Please remove all commercial language from your manuscript and use generic terms instead. All commercial products should be sufficiently referenced in the Table of Materials. I do not think there is any commercial language in the manuscript.
4. Please provide a legend for each supplemental video. The legends have been provided.

Response to Reviewers:
We thank the reviewers for their comments. Below are the point-by-point responses to the reviewers.

Change in title:
We have decided to change the title to "Bead movement based computational framework for analysis of 3-dimensional biofilm material heterogeneity". The addition of "3-dimensional" sets the technique apart from microrheology that analyzes bead movement in 2D. The addition of the word heterogeneity better reflects how these differences can be heterogeneous within different parts of the same biofilm.

Point by point response to the reviewers:
Reviewers' comments:
Reviewer #1:
Manuscript Summary:
The authors describe a method for analyzing and quantifying the movement pattern of 1μm glyoxylate beads added to bacterial biofilms grown in multiwell plates after several washing procedures. Then they pretend to use the movement patterns of the beads to quantitate differences in material properties of biofilms.

Major Concerns:
The washing procedures introduce un-controlled steps in the protocol. The beads are post-added and probably stuck to the biofilm surface and the sealing of the coverslip is expected to significantly alter the biofilm material properties — the issue is not addressed. The material properties the authrors are talking about are not defined. The measurements are so scatterred that I don't understand how they can be interpreted in terms of brownian motion with a linear dependence of the MSD with time. The reviewers comments have been broken down into the following subjects:

Pretending to use the movement pattern to quantitate differences in material properties and the material properties are not defined (reviewer 2) and differences in microrheology (reviewer 2). This statement may arise from different application of terminology arising from different fields. The 4D videos over 20 minutes played at approximately 100X revealed visually different overall material properties of the biofilms. Some biofilms are more homogeneous and show a viscous fluid-like movement versus biofilms that appeared rigid

with no visible movement as well as curli mutant biofilms that had a mixture of viscous and rigid areas (heterogeneous biofilms). These properties are likely derived from different material properties. These material properties would include, the contribution of amyloids shown for the Enterobacteriaceae biofilms, as well as cell density contributions, and chemistry differences. While microrheology tracks can be used to analyze viscoelastic properties in 2D, there was not a good way to quantitate these clearly different overall behaviors in 3D. 3D tracking over time (4D) is important for properties like the movement of bacteria (proxy for the carboxylate beads with bacteria-like charge) or antibiotic movement through 3D structures. We can track bead movements over 20 minutes and generate trajectories for each bead in the biofilm. The bounding box and velocity of the bead movement corresponds to visual inspection of the bead movement when observing the beads in the video associated with more fluid-like (viscous) and more rigid regions of the biofilm. While, we agree, we are not directly providing quantitative measurement of elastoviscosity of the biofilms, we are providing a method for quantitating observed visual differences as well as a method for tracking movement of particles through biofilms with different material properties.

Washing steps: The washing steps are necessary to remove our bacterial growth medium that has a strong green channel autofluorescence and to move unassociated beads from the biofilm. The background of unassociated beads would increase the data set. This was mentioned in step 2.1.2 as an optional wash step. We have added a discussion about the technical challenges of the wash steps to the critical steps. Our technique is easily applicable to biofilms that do not need to be washed. This explanation was added Lines 583-586.

Post adding of the beads: We choose to use excess beads and remove unassociated beads by washing to maximize the associated beads to get the most accurate characterization of the observed regions. We agree that the beads associated with the biofilm are in some sense "stuck", they are associated with the biofilms and do not easily wash off. If the beads were moving through with no association that would be more a measure of penetrance than biofilm material property. The choice of carboxylate beads with the approximate charge of bacterial cells was intentional as a proxy for movement of things such as bacteria through these biofilms. The addition of beads during biofilm growth could be an interesting way to get the beads "trapped" in the biofilm rather than associated with the biofilm for a more accurate measure of biofilm movement without risk of disassociation of the beads in a viscous biofilm. A section describing this has been added to the Modifications and Future Applications (Lines 603-616).

Mounting on coverslip: We agree a mounted coverslip may introduce artifacts, which is the reason that throughout the manuscript, we presented data in each figure comparing the mounted *E. faecalis* to one in an optic bottom well (*E. faecalis* bottom). We found them to be very similar to the mounted coverslip in each figure (*E. faecalis*). Then in the critical steps, we discussed the limitations we did note when using a mounted coverslip. Finally, the use of coverslips was listed as the biggest technical challenge in the discussion section. The reason the mounted coverslip was used in our studies is because of the technical challenges with some aerobic pellicle biofilms, that even in the hands of Enterobacteriaceae experts, could

not be properly grown in an optic bottom plate or in a flow cell that would allow imaging without mounting (this was discussed under the heading of "bounding box analysis").

"I don't understand how they can be interpreted in terms of brownian motion with a linear dependence of the MSD with time" To analyze the general movement pattern of beads we computed the mean square displacement for each bead over time. Given that a linear time profile of the MSD means that the particle is moving diffusively we performed a least squares fit to all trajectories and evaluated the weight of the second order term. If the second order term was significantly smaller than the first order term, we concluded that the MSD develops linearly over time. This could be confirmed for the analyzed data, bringing us to the conclusion that beads move passively by diffusion through the medium.

Reviewer #2:
Manuscript Summary:
Buttaro and Queisser describe a technique to probe biofilm structural properties by flowing 1 um beads and analyzing their paths. The method is then applied to the study of the biofilms formed by Enterococcus faecalis, Salmonella enterica serotype Typhimurium and Escherichia coli. Bead trajectories are analyzed and reconstructed using the Mosaic plugin in Image J and movement data. In this work the authors present the workflow from data collection to the analysis and present results regarding biofilm material properties related to the presence of curli.

The manuscript is well written and the procedure is interesting. I recommend to follow up with the video, after the following comments are addressed.

Major Concerns:

- The description of the procedures to prepare the sample for imaging is difficult to follow with just the description. Please make sure that in the video this part is well explained and shown. We added some more details to the various steps of the protocol to try and paint a clearer picture of each step. We agree that some of this may require a video to clarify the written descriptions. Lines 134-149.

- Lines 92-92: "reveal the material properties responsible for movement of beads we observed in biofilms that were not under flow" is routinely done by microrheology (see [1,2]), so I would not sell this as an element of novelty of the technique. I would suggest to discuss the technique in light of results obtained with microrheology.
We had references 1 and 2 in our version of the manuscript but we had not appropriately discussed them. One of the major differences is microrheology is a 2D particle tracking technique. Viscoelasticity of different regions of a biofilm could be determined by 2D microrheology at different Z positions. However, this technique does not allow contiguous tracking of particle movement through 3D biofilms, which is the goal of our technique. We modified the Introduction Lines 79-85 and added 3D to the Title to better discuss these differences.

We also more carefully explained that the differences we observed are due to movement in three directions is based on material properties, cellular density, interactions of the beads with the chemistry of the matrix and 3D heterogeneity. Lines 412-413.

- Would it be possible to implement this procedure in microfluidic channel, without displacing the biofilm sample? This would allow avoiding the problems described at lines 343-344. As also mentioned in the Discussion, the fact of not being in-situ is the main limitation of the technique.

Absolutely, this was briefly mentioned in the original introduction and has been emphasized there and a section has been added to the modifications and future applications. Line 106 and 602-607

- Line 358: Do the authors take the image of a single layer? This point should be precisely discussed and the influence of the 2D vs 3D geometry on the results should be carefully discussed.

We use the 3D data set for our analysis. Below are two visualizations of the 3D trajectory of 2 beads with its coordinates in μm. In the case of this bead, from the *E. coli* biofilm moved 0.04 μm in Z, 0.4 μm in Y and 0.4 μm in X. In the case of the *E. faecalis* bead on the right it moved 7 μm in Z, 16 μm in Y and 12 μm in X. The trajectory visualization is not part of the current tool because of limitations in bead trajectory stitching. The use of 3D has been clarified throughout the manuscript and added to the title.
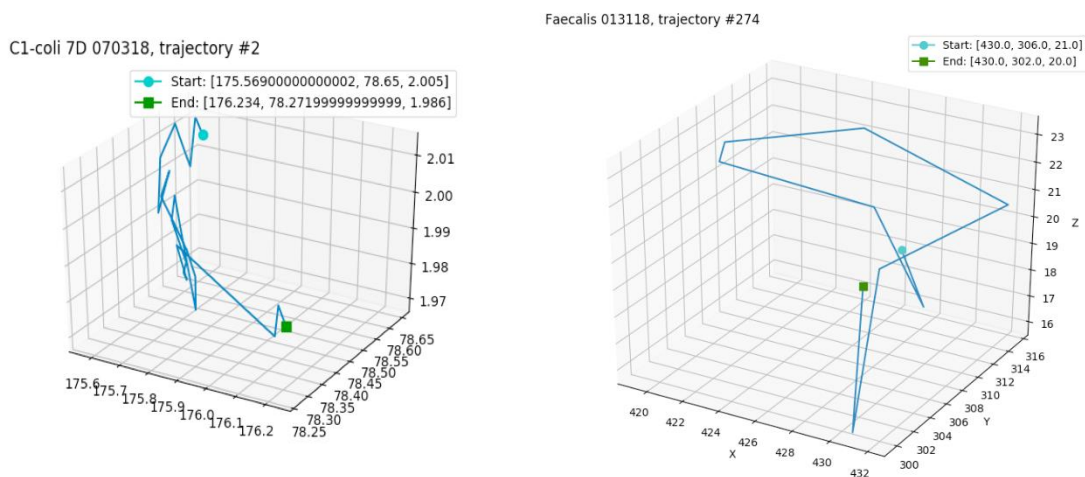
- Line 390: What could be the impact of the particle surface properties on the results?

Good point. That has been added to the manuscript Lines 411-412.

- The optical quality of the figures is quite poor. I suspect it could be due to the PDF preparation, but the problem should be addressed in the final version.

We are not sure what happened here since JoVE assembled the final pdf. We will make sure the optical quality is good for publication.

Minor Concerns:

- Lines 72-73: The authors say that the target for their research is the movement of plasmids- they should say explicitly that they are transported by bacteria, and so basically they target the motion of bacteria in the biofilm.

We are using 3 different fluorescent wavelengths tagging, donors, recipients, and the plasmid itself to follow movement of the added donor cell to the recipient population, docking, and plasmid transfer.   This has been clarified Lines 110-111.

- Line 130: Could the growth condition of each biofilm be clarifies for the reproducibility of the results?
Growth conditions have been added to the manuscript, we apologize for the oversight. Step 1.2 Lines 147-149.

- Line 158: What is the Crimson bead concentration? The procedure described in 2.1.3 is not clear.
The concentration of the beads was $2x10^7$/ml as outlined in Step 2.1.1. In Step 2.1.3 for 24 well coverslip biofilms 1 ml was added giving a total of $2x10^7$ beads and for the 96-well optic bottom biofilms 0.2 ml was added giving a total of $4x10^6$ beads. This clarification was added to steps 2.1.3. Lines 177-179.

- Line 412: Could some details about the procedure used to calculate the cell density be given?
The cellular density was computed by averaging the Syto9 voxel data over the bounding box of each trajectory edge. Thus, the bead velocity can be weighted by the edgewise (local) cell densities. This was added to the manuscript Lines 438-441.

These were included but not well discussed in the original version.
[1] S. C. Chew, B. Kundukad, T. Seviour, J. R. C. Van der Maarel, L. Yang, S. A. Rice, P. Doyle, and S. Kjelleberg, Dynamic Remodeling of Microbial Biofilms by Functionally Distinct Exopolysaccharides, MBio 5, e01563 (2014).
[2] A. Birjiniuk, N. Billings, E. Nance, J. Hanes, K. Ribbeck, and P. S. Doyle, Single Particle Tracking Reveals Spatial and Dynamic Organization of the Escherichia Coli Biofilm Matrix, New J. Phys. 16, (2014).

Reviewer #3:
Manuscript Summary:
Buttaro et al. is using time lapse fluorescence confocal microscopy looking at fluorescent bead movement within a biofilm. They have also created a workflow to monitor the movement using various software. The technique is interesting and allows for a unique way to study the viscoelastic properties of microbial communities. This technique seems appropriate for publication in JOVE, but there are several minor things in the manuscript that need to be addressed prior to publication.

Major Concerns:
Lines 63-64. The authors state that they were unable to see any amyloids present in E. faecalis. What staining method was performed to look for amyloids? If using Congo Red from the (9) citation, this is not a reliable stain for amyloids. Khurana et al. 2001 J Biol Chem.
We did use Congo Red at the time this experiment. However, in our case, since we did not see staining, we felt this was sufficient for these studies. Had we seen staining, the experiments would have been repeated with Congo Red FSB (Reichardt 2018) to provide better specificity for amyloid.

Lines 53-68. This paragraph appears to be making the argument that a major difference between Enterobacteriaceae and E. faecalis biofilms is the presence of amyloids. I think it is incorrect to say that the difference between E. faecalis biofilm and others are amyloids. It is an exhaustive process to find amyloids within a biofilm, and the authors did not prove conclusively that this isolate does not produce an amyloid in this biofilm model. Additionally, there are many differences in extracellular DNA, cell wall, extracellular sugars, and proteins between this Gram-+ isolate and the Enterobacteriaceae evaluated in this study that could all effect the rigidity or physical properties of the biofilm. This means there are too many differences for the authors to say the main difference in viscoelasticity in the biofilm is due to the presence or absence of an amyloid. The authors should more generally talk about the differences in the biofilms. Comparing E. coli and S. enterica WT and curli mutants IS a direct way to elucidate the role of microbial amyloids in viscoelasticity in this assay.

This is what we meant to say and did not say it well at all. This section has been reworded. Lines 64-77.

Minor Concerns:
Line 45-46. Curli are not just specific for Enteric bacteria. Dueholm et al. 2012 Plos one
This paper has been included in the references and the statement broadened. Lines 51-52.

Lines 60-62. The authors state that their strain does not have the gene encoding Esp. The authors should state what bioinformatic method was used to ensure that esp is not present.
We just used a standard BLASTn and BLASTp searches and it has been added to the manuscript. Line 70

Line 64, do the authors mean "E. faecalis" not "S. Typhimurium"?
We did mean *E. faecalis*. Thank you.

The authors refer to the other evaluated strains by their species names (E. coli, E. faecalis), but consistently use S. Typhimurium instead of S. enterica. There should be consistency in nomenclature used in the manuscript.
S. Typhimurium is a standard way to refer to *S. enterica* serovar Typhimurium because *S. enterica* serovars are significantly different. The original paper containing this technique was published with C. Tukel, an expert on *S.* Typhimurium, who used this nomenclature in the manuscript from which many of these figures are described.

The figures are very pixelated and difficult to see. They should be re-captured.
We will make sure the final pictures are not pixelated. Thanks.

Figure 2B and D. Were these experiments stopped short of the rest of the experiments? There should be consistent data capture between runs that are being compared.
The runs were of equal length. The trajectory lifespans are shorter because the beads either make large movements that cannot be stitched, or the beads disassociate and reassociate with the biofilm. Thus, no one trajectory was followed for longer than 10 minutes although beads could be observed associated with the biofilm the entire time. This is discussed in lines 385-394.

The E. coli WT and curli mutant videos are taken from different angles. This can also be seen

in Figure 1B. All the videos and stills should be at consistent angles, zoom, and timeframes to allow for proper comparison.

An important aspect of the images is to show the beads associated with the biofilm. Due to the presence of heterologous rigid structures, which can obscure the beads, different orientations are necessary to make sure the beads are visible.

The authors don't specifically mention all the subfigures within the text. I'm not sure if this is JOVE specific or not, but Figure 1a, 1b, 1c are not mentioned in the text.

These were accidently omitted from the first version. Fig. 1A is at line 87. Fig. 1B in line 319 for the description of the representative results.

Fig. 3I and J are mentioned in the text prior to 3a. Also, the figure 3 legend discusses 3c prior to 3a.

This reference to Fig. 3I and 3J was moved to a more appropriate section of the manuscript around line 380 at the conclusion of the bounding box section.

One of the most interesting things about this data, that the authors don't really discuss is the median vs. mean displacement seen in the WT and curli mutants. The mean data (Fig 3J) shows that curli are important for decreasing overall movement of these fluorescent objects in the biofilm. But, they have almost identical medians (Fig. 3B), showing that any particular location in the biofilm can halt movement of physical objects to a similar degree, but the presence of the amyloid almost eliminates all areas of the biofilm that allow for a physical object to move. I think this piece of data is quite intriguing and it isn't discussed in the manuscript.

We agree, the bounding box volumes were consistently small (0-10 μm^3) even in low density regions of the biofilm. This observation is consistent with our previous observations that curli can be present in low cell density regions of the biofilm. The small bounding box volume data in Figure 3B confirms this observation and well as the low mean square displacement in Fig. 3J. This has been added to the manuscript at Lines 371-373.